HHS Public Access

Author manuscript

J Immunol. Author manuscript; available in PMC 2020 January 15.

Published in final edited form as:

J Immunol. 2019 January 15; 202(2): 428–440. doi:10.4049/jimmunol.1601395.

Dual oxidase 1(Duox1) regulates primary B cell function under the influence of IL-4 through BCR-mediated generation of hydrogen peroxide

Ryuichi Sugamata[*], **Agnes Donko**[*], **Yousuke Murakami**[†], **Howard Boudreau**[*], **Chen-Feng Qi**[†], **Jaeyul Kwon**[*], and **Thomas L. Leto**[*,‡]

[*]Molecular Defense Section, Laboratory of Clinical Immunology and Microbiology, National Institute of Allergy and Infectious Diseases, National Institutes of Health, 12441 Parklawn Drive, Rockville, MD 20852, USA.

[†]Pathology Core, Laboratory of Immunogenetics, National Institute of Allergy and Infectious Diseases, National Institutes of Health, 12441 Parklawn Drive, Rockville, MD, USA.

Abstract

Engagement of the B cell receptor (BCR) with antigens triggers signaling pathways for commitment of B-lymphocyte responses that can be regulated, in part, by reactive oxygen species (ROS). To investigate the functional relevance of ROS produced in primary B cells, we focused on the role of the hydrogen peroxide generator Duox1 in stimulated splenic B cells under the influence of the T_H2 cytokine, IL-4. We found that H_2O_2 production in WT and Nox2-deficient $CD19^+$ B cells was boosted concomitant with enhanced expression of Duox1 following co-stimulation with BCR agonists together with IL-4, whereas stimulated $Duox1^{-/-}$ cells showed attenuated H_2O_2 release. We examined whether Duox1-derived H_2O_2 contributes to proliferative activity and Ig isotype production in $CD19^+$ cells upon BCR stimulation. $Duox1^{-/-}$ $CD19^+$ B cells showed normal responses of Ig production, but a higher rate of proliferation than WT or Nox2-deficient cells. Furthermore, we demonstrated that the H_2O_2 scavenger catalase mimics the effect of Duox1 deficiency by enhancing proliferation of WT $CD19^+$ B cells *in vitro*. Results from immunized mice reflected the *in vitro* observations: T-cell independent antigen induced increased B cell expansion in GCs from $Duox1^{-/-}$ mice relative to WT and $Nox2^{-/-}$ mice, whereas immunization with T cell dependent or independent antigens elicited normal Ig isotype secretion in the Duox1 mutant mice. These observations obtained both by *in vitro* and *in vivo* approaches strongly suggest that Duox1-derived hydrogen peroxide negatively regulates proliferative activity but not Ig isotype production in primary splenic $CD19^+$ B cells.

[‡]Corresponding author: Thomas L. Leto, Ph.D, Molecular Defense Section, Laboratory of Host Defenses, National Institute of Allergy and Infectious Diseases, National Institutes of Health, 12441 Parklawn Drive, Rockville, MD, USA. Telephone: 301-402-5120, Fax: 301-480-1731, tleto@nih.gov.

Disclosures

The authors have no financial conflicts of interest.

Keywords

ROS; Duox1; H_2O_2; $CD19^+$ B cells; BCR; IL-4; BCAP; RGS16; CD40; T cell dependent (TD); T cell independent (TI)

Introduction

The strength of signaling pathways triggered by engagement of B cell antigen receptors (BCR) is critical for the commitment to B cell proliferation and differentiation for adaptive immune responses (1, 2). Crosslinking of BCR by antigens initiates activation of receptor proximal protein tyrosine kinases, such as Syk, Lyn, and rapid downstream phosphorylation of several tyrosine kinase substrate proteins, including Btk, phospholipase-Cγ2 (PLCγ2) and Akt kinase (3). On the other hand, BCR stimulation also recruits inhibitory regulators of tyrosine phosphorylation (protein tyrosine phosphatases; PTPs) such as Src homology region 2 domain-containing phosphatase 1 (SHP-1), which binds to immunoreceptor tyrosine-based inhibitory motifs (ITIMs) on CD22 for negative regulation of BCR signaling (4). Therefore, transmission of BCR signaling is strictly controlled by antagonistic feedback systems.

Reactive oxygen species (ROS) such as hydrogen peroxide (H_2O_2) have been considered potent inhibitors of PTPs in lymphocytes because cysteine residues in their catalytic sites can be readily and reversibly oxidized (3). ROS generation has been shown in B lymphocytes. Over 20 years ago, Kanegasaki's group first established that one of the NADPH oxidase family members, Nox2 (originally designated as the cytochrome b_{558} β-subunit or $gp91^{phox}$) is constitutively expressed on the human B cell surface and that it generates superoxide anion ($O_2\cdot^-$) following cell stimulation, similar to the respiratory burst of phagocytic cells required for microbial killing (5). Interestingly, recent work has shown that phagocytic $CD19^+$ B cells isolated from the mouse peritoneal cavity also exhibit Nox2-dependent microbicidal activity (6). It was suggested initially that $O_2\cdot^-$ produced by Nox2 is not essential for B cell development and differentiation because chronic granulomatous disease (CGD) patients lacking Nox2 activity were not recognized with any B cell dysfunction. However, more recent work indicated that CGD patients have reduced memory and increased naïve B cell counts which may affect secondary antibody responses (7–9). Studies in mice examining the relationship of Nox2-derived $O_2\cdot^-$ to primary B cell responses used splenic B cells from Nox2-deficient or Neutrophil cytosolic factor 1 ($Ncf1/p47^{phox}$)-deficient mice that are functionally Nox2 deficient (10, 11). These studies indicated Nox2 contributes to an early phase of superoxide $O_2\cdot^-$ generation in response to BCR stimulation, however, the Nox2 defects in these models do not appear to affect normal B cell development and maturation significantly.

Dual oxidase (Duox) molecules are among Nox family NADPH oxidase members that have been associated with signaling pathways in lymphocytes. Duox1 and Duox2 exhibit calcium-dependent generation of hydrogen peroxide (H_2O_2) produced directly from a superoxide intermediate due to activity of their unique extracellular peroxidase-like domains (12, 13). In T cells, H_2O_2 derived from Duox1 following T-cell receptor (TCR) stimulation

inactivates PTP activity of SHP-2, which enhances proximal TCR signaling through enhanced phosphorylation and activation of ZAP-70 molecules (14). A similar BCR signaling feedback system involving Duox1-derived H_2O_2 was proposed in B lymphocytes. Using A20 murine B lymphoma cells, this study suggested that H_2O_2 produced by Duox1 following BCR stimulation enhances intracellular calcium signaling and a positive-feedback loop of Lyn phosphorylation by negatively regulating PTP activity of SHP-1 (15). On the other hand, it has not been clear from these studies whether Duox1-derived H_2O_2 contributes to later phase intrinsic B cell activities, including cell proliferation or IgG production.

The function of Duox1 is boosted by T_H2-type cytokines in several cell types. IL-4 and IL-13 have the ability to promote production of Duox1 and increase H_2O_2 generation for innate immune defense in human primary respiratory epithelial cells and pulmonary carcinoma cell lines (16, 17). Furthermore, airway T_H2-based innate immune responses to allergic asthmatic challenges are diminished in mice deficient in Duox1 or Duoxa (18, 19). An enhancement of the Duox1-H_2O_2 axis by IL-4 or IL-13 was also observed in human primary keratinocytes (20). Here, knocking-down Duox1 alters expression of transcription factors and phosphorylation of STAT6 induced by T_H2-type cytokines due to decreased H_2O_2 production. Together, these observations indicate that Duox1 and the H_2O_2 it generates participate in a positive feedback loop of T_H2-type cytokine signaling in keratinocytes and respiratory epithelium.

T_H2-type cytokines are well-known essential mediators of B cell function and development. The relationship between Duox1 and T_H2-type cytokines has not yet been examined in the primary B cells, but should be approached for a better understanding of signaling in developing B cells. In this study, we determined that Duox1 affects BCR stimulation of primary splenic B cells specifically under the influence of the T_H2-type cytokine IL-4. Following this concept, ROS production mediated by Duox1 in the B cells was examined by comparing cells from wild type and Duox1 mutant mice in order to determine whether ROS play a regulatory role in B cell signaling. We further aimed to uncover downstream functional consequences of Duox1-derived ROS in primary B cell activities.

Materials and Methods

Mice

The mice between the ages of 8 and 12 weeks were used for experiments. B6 mice (000664; C57BL/6J) and B6 background gp91^{phox}-deficient mouse (002365; B6.129S-Cybbtm1Din/J) were purchased from The Jackson Laboratory (Bar Harber, ME, USA). The Duox1-deficient mice were established on a B6 background by retroviral-based gene-trapping methodology (21, 22) and were kindly provided by Dr. M. Geiszt (Semmelweis University, Budapest, Hungary). Mice were housed with a standard diet and given water in a specific pathogen-free facility, according to National Institutes of Health guidelines. Animal use was approved by the NIAID Animal Care and Use Committee.

B cell characterization by flow cytometry analysis

Fluorophore-conjugated Abs directed against the following surface markers were used: B220 (RA3–6B2), CD23 (B3B4), CD69 (H1.2F3), CD93 (AA4.1) and CD86 (GL-1) from eBioscience (San Diego, CA, USA); CD19 (1D3) from BD Pharmingen (San Diego, CA, USA); IgM (goat polyclonal F(ab')$_2$, μ chain specific) from Jackson ImmunoReseach (West Grove, PA, USA). B cell populations from the spleen and bone marrow (BM) were stained for 30 minutes on ice with anti-CD23-FITC, anti-IgM-PE-Cy7, anti-CD93-allophycocyanin (APC), anti-B220-APC-eFlour 780, and B cell subpopulations from each mouse strain were investigated on an LSR II flow cytometer (BD Biosciences, San Jose, CA, USA) by Allman's protocol (23). Dead cells were identified and excluded by propidium iodide staining (BD Pharmingen). Flow cytometry data were analyzed with FlowJo software version 10 (Tree Star, Ashland, OR, USA).

B cell purification

Total splenic cells were collected from spleens by homogenization and the single cell suspensions were treated with lysis buffer (Lonza, Basel, Switzerland) to eliminate erythrocytes. CD19$^+$ B cells were positively-selected by magnetic-activated cell sorting (MACS) of total splenic cell suspensions using microbeads and MACS LS separation columns (Miltenyi Biotech, San Diego, CA, USA), according to the manufacturer's instructions.

ROS assay

ROS production in the vicinity of BCR was detected by use of anti-IgM F(ab')$_2$ conjugated to OxyBURST Green H_2DCFDA, succinimidyl ester (Invitrogen), as described in previous reports (11, 24). A million CD19$^+$ cells were re-suspended in phenol red-free HBSS (Ca/Mg salts plus) supplemented with 10 mM HEPES (Gibco) and 1% FBS. Cells were incubated with 20 μg of OxyBURST Green-conjugated anti-IgM F(ab')$_2$ for 30 min on ice, then were washed and activated at 37^o C for 10 min. ROS production was measured by detecting 488 nm fluorescence emission by flow cytometry using LSR II using DIVA software.

The purified CD19$^+$ cells were stimulated by goat anti-mouse IgM F(ab')$_2$ fragment (SouthernBiotech, Birmingham, AL, USA), mouse IL-4 (R and D systems, Emeryville, CA), or IL-13 (R and D systems) in complete RPMI 1640 medium supplemented with 10% FBS (Atlanta Biologicals, Flowery Branch, GA, USA), 1% Penicillin/Streptomycin (Gibco, Carlsbad, CA, USA), 5 mM HEPES (Gibco), 1% MEM non-essential amino acids (Gibco), 1 mM sodium pyruvate (Gibco), 2 mM L-Glutamine (Gibco) and 50 μM 2-Mercoptethanol for 24 h at 37° C under 5% CO_2. After the incubation, the cells were transferred into microcentrifuge tubes, then immediately double-stained in phenol red-free HBSS (Ca/Mg salts plus, 10 mM HEPES and 1% FBS) containing each 5 μM of OxyBURST Green H_2DCFDA, succinimidyl ester (Invitrogen) and CellRox (Invitrogen) for 30 min at 37°C. The cells were washed and subjected to flow cytometry analysis using LSR II and DIVA software.

B cell proliferation assay

Stimulant-induced B cell proliferation *in vitro* was analyzed by 5-(and 6)-Carboxyfluorescein diacetate succinimidyl ester (CFSE) staining methodology (Thermo Fisher Scientific, Ashville NC, USA). Purified splenic $CD19^+$ B cells were labeled with 5 mM CFSE for 10 min at 37°C. After washing, the labeled cells were resuspended at a concentration of 1×10^6 cells/ml in complete RPMI 1640 medium and were cultured with 5 μg/ml of anti-mouse IgM $F(ab')_2$ in the presence or absence of IL-4 (20 ng/ml), either with or without 1 unit/μl of catalase for 72 h at 37° C. Cells were collected and diluted fluorescence peaks of CFSE detected with each successive cell division were analyzed by flow cytometry using LSR II and DIVA software.

cDNA preparation and Quantitative real-time PCR

Total RNA was prepared from $CD19^+$ B cells using the RNeasy kit (Qiagen, Venlo, Netherlands) by treatment with RNase-Free DNase (Qiagen). The cDNA was generated with a ThermoScript reverse transcriptase (Invitrogen, Carlsbad, CA, USA). Real-time PCR was performed in a 7500 Real Time PCR System (Applied Biosystems, Foster City, California, USA) using Power SYBR Green PCR Master Mix (Applied Biosystems) reagents with specific oligonucleotide primer pairs (Supplementary Table 1). The PCR reaction conditions were 50° C for 2 min, and then 95° C for 15 s and 60° C for 1 min, repeated for 40 cycles, with hot start at 95° C for 10 min. The expression levels of each gene were normalized to that of an internal control gene, EIF3F (eukaryotic translation initiation factor 3, subunit F).

Immunizations, *in vitro* Ig production, and ELISA

Pre-immunized sera were obtained from WT, $Duox1^{-/-}$ or $Nox2^{-/-}$ mice before immunization. For T cell-independent (TI) immunizations, several groups of 3–4 mice per strain (8–10 weeks old) were injected intraperitoneally with 50 μg nitrophenyl-lipopolysaccharide (NP-LPS; Biosearch Technologies) in 200 μl PBS. Other mice were injected with100 μg NP-keyhole limpet hemocyanin (NP-KLH) precipitated with alum (Imject^R; Thermo Scientific). Immune sera were collected from mice on 7 or 8 days (TI) and 14 days (TD) after immunization.

To examine Ig isotype production *in vitro*, purified splenic $CD19^+$ B cells were re-suspended at a concentration of 1×10^6 cells/ml in complete RPMI 1640 medium and were cultured with IL-4 alone (20 ng/ml), 5 μg/ml of anti-mouse IgM $F(ab')_2$ or anti-mouse CD40 antibody (Southern Biotech) in the presence or absence of IL-4 (20 ng/ml) for 72 h at 37° C. After co-culture with stimulants, culture supernatants were collected for ELISA assays.

To measure production of each Ig-isotype in the culture supernatants, a mouse Ig Isotyping ELISA Ready-Set-Go kit (eBiosciences, San Diego, CA, USA) was used according to manufacturer's instructions using standards of mouse IgM, IgG1, IgG2a, IgG2b, IgG3 and IgA (eBiosciences). ELISA assays were performed in 96-well plates (Greiner Bio-One, Monroe, NC) from OD (490–520 nm) measurements recorded with a micro plate reader (Victor^2 1420 Multi label counter, WALLAC).

Immunohistology

Whole spleen tissues collected from immunized and non-immunized mice were fixed in 10% buffered formalin and embedded in paraffin. Tissue sections were stained either with hematoxylin and eosin (H&E) or processed for immunostaining according to standard protocols. (25). Immunostaining was performed by the avidin-biotin peroxidase or alkaline phosphatase complex (ABC) methods using the Vectastain Elite ABC kits (Vector, Burlingame, CA), according to manufacturer's instruction. Antibodies and other reagents were obtained from the following sources: rat anti-CD3 (BioRad; #MCA1477, 1:100), anti-B220 (BD Bioscience; # 553086, 1: 200), rabbit rat anti-Ki67 (Abcam; #16667 1:100), PNA-biotin conjugate (Vector; #B-1075, 1:1000) anti-IgM (Vector; #ba2020; 1:100), goat anti-PAX5 (Santa Cruz: #sc-1974, 1:750).

For quantitative analyses, 20 microscopic high power (hp; x40) fields in each case for proliferating cells with Ki67 positivity of blast cells in the germinal centers of spleens (three mice for each group to take the average number of Ki67 positives) and at low power (lp; x5) to count all germinal center with PNA reaction positivity (three mice for each group to obtain average GC numbers within spleen sections). All immunohistochemical data were analyzed by two pathologists.

Western blot analysis

$CD19^+$ B cells were washed in phosphate-buffered saline and were suspended in RIPA buffer (Sigma-Aldrich, St. Louis, MO) containing protease inhibitor and phosphatase inhibitor cocktails (Sigma-Aldrich). After incubation on ice for 15 min, supernatants were collected by centrifugation as whole-cell protein extracts and were quantified by Bradford assays using Coomassie plus protein assay reagents (Thermo Fisher Scientific, Pittsburgh, PA). Twenty to 30 μg of the whole-cell extracts were resolved electrophoretically on 4-to-12% Bis-Tris NuPAGE gels (Invitrogen) then transferred on polyvinylidene difluoride membranes (Life Technologies). Immunoblotting was performed with commercially available antibodies: mouse anti-phosphotyrosine monoclonal antibody (Millipore, Billerica, MA, USA), mouse anti-human/mouse RGS16 monoclonal antibody (4E5) (Abcam), rabbit anti-mouse Akt polyclonal antibody (Cell Signaling Technology, Danvers, Massachusetts, USA), anti-mouse phospho-Akt (Ser473) polyclonal antibody (D9E) (Cell Signaling Technology), Goat anti-human/mouse BCAP/PIK3AP1 polyclonal antibody (Novus Biologicals, Littleton, CO USA), rabbit anti-human/mouse GAPDH polyclonal antibody (Trevigen, Gaithersburg, MD, USA). Some membranes were stripped using restore PLUS Western Blot Striping Buffer (Thermo Fisher Scientific) and re-probed.

Statistical analysis

All data sets in each experiment were subjected to normality test by Shapiro-Wilk test. Based on the results, statistical differences were assessed by Student's *t*-test, Mann-Whitney *U*-test, Kruskal-Wallis test, Friedman test or Two-way ANOVA using GraphPad Prism software version 5 (GraphPad software, Inc., La Jolla CA, USA).

Results

Duox1 deficiency does not influence B-cell development, NADPH oxidase expression patterns or early-phase BCR-stimulated extracellular H_2O_2 production.

In initial experiments, we assessed the influence of Duox1 deficiency on B cell homeostasis by analyzing B cell populations isolated from BM and spleen. The absence of Duox1 in mice resulted in a normal distribution of each B cell subset detected in populations isolated from BM and spleen when compared with those from WT mice (Figure 1a).

We investigated the expression patterns of all Nox/Duox family member transcripts in freshly isolated splenic $CD19^+$ B cells handled under non-stimulatory conditions. The magnetically isolated $CD19^+$ cell populations from spleen were confirmed for CD19 expression on their cell surface, showing 97.5% CD19-positivity within this sorted population (data not shown). No differences in the relative expression of Nox1, 2, 3, 4 and Duox2 transcripts in splenic $CD19^+$ B cells were detected between WT and Duox1-deficient mice (Figure 1b). Although Duox1 transcripts were detected in the cells of mutant mice at normal levels (Figure 1b), a previous report characterizing this mutant strain demonstrated that the Duox1-targeted frame-shifted transcript is not translated into a detectable or functional protein (22). These observations indicate that the absence of Duox1 does not influence B cell development or expression levels of other Nox family transcripts, at least under healthy, unstimulated conditions.

We detected an early phase (at 10 min) of ROS production in the vicinity of stimulated BCR using OxyBURST Green succinimidyl ester (DCFDA-SE) conjugated to anti-IgM $F(ab')_2$ as both an agonist and redox-sensing probe. BCR stimulation increased the mean fluorescence intensity (MFI) detected by OxyBURST Green on anti-IgM $F(ab')_2$ in WT $CD19^+$ B cells (Figure 1c). Duox1-deficient cells showed OxyBURST MFI values comparable to that of WT cells, whereas Nox2-deficent ($gp91^{phox}$-deficient) cells showed remarkably lower signals following BCR stimulation (Figure 1c), consistent with earlier studies on Nox2-deficient mice (11). Addition of horseradish peroxidase (HRP) catalyzed enhanced oxidation of DCFDA on the anti-IgM $F(ab')_2$ by H_2O_2 produced by stimulated $CD19^+$ B cells, resulting in greatly enhanced fluorescence signals (>15-fold relative to the assays lacking HRP) from cells from WT and $Duox1^{-/-}$ mice (Figure 1c). These findings indicated this early-phase signal is in large part attributable to extracellular H_2O_2 release from Nox2 in the vicinity of stimulated BCR.

IL-4 increases BCR-stimulated extracellular H_2O_2 signals from Duox1, whereas $O_2{\cdot}^-$ signals are unaffected in $Duox1^{-/-}$ $CD19^+$ B cells

In order to explore factors that could affect gene expression of Duox1, we investigated whether the expression of Duox1 in splenic $CD19^+$ B cells is changed by stimulation with anti-IgM $F(ab')_2$ in combination with T_H2-type cytokines. Stimulation with anti-IgM $F(ab')_2$ or IL-4, or costimulation of anti-IgM $F(ab')_2$ and IL-4 for 6 hours did not alter Duox1 expression (Supplementary Fig. 1a), whereas costimulation with anti-IgM $F(ab')_2$ and IL-4 for 24 h induced significantly higher expression of Duox1 (Figure 2a). To consider other possible ROS sources, we examined expression patterns of all other NADPH isoforms

at this time point. Gene transcript levels of Nox1, Nox2, Nox3, Nox4 and Duox2 were not influenced by any stimulants for 24 h (Figure 2a). Treatment with another T_H2-type cytokine, IL-13, did not enhance Duox1 gene expression in $CD19^+$ B cells after 24 h costimulation (Supplementary Fig. 1b). The enhanced Duox1 expression by co-stimulation with BCR plus IL-4 was not maintained at 48 or 72 hours post-stimulation (Supplementary Fig. 1a).

We designed strategies for simultaneous detection of hydrogen peroxide (H_2O_2) and superoxide ($O_2\cdot^-$) in cells at 24 hours post-stimulation, when Duox1 expression is maximally enhanced. For these parallel ROS assays, we used OxyBURST Green-succinimidyl ester and CellRox dye reagents for double staining because cell surface labeling with OxyBURST Green detects Duox1-derived H_2O_2, whereas CellRox preferentially react with intracellular $O_2\cdot^-$ produced by Nox2. In comparison to unstimulated cells, 24 hours stimulation with anti-IgM $F(ab')_2$ alone increased the MFI of OxyBURST Green on WT $CD19^+$ B cells (Figure 2b, upper panel). Costimulation with anti-IgM $F(ab')_2$ and IL-4 remarkably induced the OxyBURST fluorescence in WT and Nox2 mutant B cells, while the signal detected from Duox1-deficient cells was considerably lower (Figure 2b, upper panel). Meanwhile, production of $O_2\cdot^-$ sensed by CellRox also increased following stimulation with anti-IgM $F(ab')_2$, and the signal was further enhanced by additional IL-4 in both WT and Duox1 mutant $CD19^+$ B cells (Figure 2b, lower panel). CellRox fluorescence was comparable between WT and $Duox1^{-/-}$ $CD19^+$ B cells, but was attenuated in Nox2 mutant cells co-stimulated with anti-IgM $F(ab')_2$ and IL-4 (Figure 2b, lower panel). Similar trends in ROS production were detected using OxyBURST Orange-succinimidyl ester and CellRox in both WT and Duox1 mutant B cells following costimulation (Supplementary Fig. 2), whereas treatment with IL-13 in place of IL-4 did not increase H_2O_2 signals (Supplementary Fig. 1c). These observations indicate that the H_2O_2 signal increases following 24 hours co-stimulation by IL-4 and BCR are Duox1 dependent, whereas the $O_2\cdot^-$ signal is unaffected by Duox1 deficiency.

Duox1-deficiency enhances B cell activators and signaling mediators.

We examined whether there are any detectable signaling pathway differences between WT and mutant $CD19^+$ B cells within 24 h of stimulation (Figure 3). We compared the total cellular tyrosine phosphorylation status of WT, $Duox1^{-/-}$ and $Nox2^{-/-}$ $CD19^+$ B cells at 1 min, 5 min and 24 hours post-stimulation by Western blotting (Figure 3a). The phosphorylation was greatly reduced at 5 min in the B cells during early responses by stimulation anti-IgM $F(ab')_2$ alone. This supports findings reported by Singh and collaborators (15) that phosphorylation of more than 60% among phosphoproteins was transiently attenuated at 5 min during fragment anti-Ig stimulation. Co-stimulatory condition by anti-IgM $F(ab')_2$ and IL-4 for 24 h led to several differences in phosphorylation responses in the B cells from WT and mutant mice, particularly in the $M_r \sim 60$ kDa range. Surface expression of an early B cell activation marker, CD69, was enhanced in $Duox1^{-/-}$ $CD19^+$ B cells by co-stimulation with anti-IgM $F(ab')_2$ and IL-4 for 6 h, but was comparable with WT cells up to 12 h post-stimulation (Figure 3b). Another activation marker, CD86, showed comparable expression levels between WT and Duox1-deficient cells at 12 and 18 h.

At 24 hours post-stimulation, we observed no significant changes in expression of the BLNK adaptor molecule in Duox1$^{-/-}$ *versus* WT D19^{+} B cells by treatment with IL-4 or anti-IgM F(ab')$_2$ alone, or in combination (Figure 3c). In contrast, BCAP, another adaptor molecule for BCR signaling was relatively increased by each stimulus. Interestingly, the regulator of G-protein signaling 16 (RGS16) gene transcript level was increased in Duox1$^{-/-}$ CD19^{+} B cells by stimulation with either anti-IgM F(ab')$_2$ alone, or combination of anti-IgM F(ab')$_2$ and IL-4 (Figure 3c). The increase of BCAP and RGS16 transcripts was reflected in the levels of protein production by the combination (Figure 3d). Basal production and phosphorylation of Akt were further examined, however, we did not observe any differences in total Akt production levels or its phosphorylation at residue Ser-473 in Duox1$^{-/-}$ cells in comparison to those from WT or Nox2$^{-/-}$ mice (Figure 3e). In all three mouse strains, we observed enhanced p-Akt levels either in response to anti-IgM F(ab')$_2$ stimulation alone or in combination with IL-4 treatment.

Duox1 deficiency influences proliferative activity, but not Ig production by CD19^{+} B cells.

To approach other functional consequences of H_2O_2 generated by Duox1 in splenic CD19^{+} B cells, we next focused on intrinsic B cell functions. Duox1-deficient CD19^{+} B cells stimulated by anti-IgM F(ab')$_2$ alone for 3 days showed higher proliferative activity, and additional IL-4 treatment further enhanced this effect in WT cells (Figure 4a). We quantified actual cell numbers in each proliferative cycle peak within whole divided CD19^{+} B cells using counting micro-beads as a standard in the CFSE-based assay. Duox1-deficient cells showed higher counts than WT cells in each division cycle 1, 2, or 3 in response to a single anti-IgM F(ab')$_2$ stimulus (Figure 4b, left panel). Following co-stimulation with anti-IgM F(ab')$_2$ and IL-4, both Duox1$^{-/-}$ and Nox2$^{-/-}$ CD19^{+} B cells showed significantly increased counts within division cycle 2 and 3, however the counts of Nox2 mutants were lower than those of Duox1 mutant cells (Figure 4b, right panel). In terms of total divided cells, co-stimulation with anti-IgM F(ab')$_2$ and IL-4 led to higher proliferative rates of CD19^{+} B cells than with single stimulation with anti-IgM F(ab')$_2$ in WT (Figure 4c). The proliferative capacity of Duox1-deficient cells greatly exceeded that of WT, whereas Nox2 mutants showed the second-largest proliferation increases following co-stimulation (Figure 4c). With each stimulus, significant differences in dead cells, detected as propidium iodide-positive (PI^{+}) events, were not seen between WT and Duox1$^{-/-}$ CD19^{+} B cells, however, PI^{+} events were statistically increased in Nox2$^{-/-}$ cells following stimulant-induced proliferation (Figure 4d).

Based on the above cell proliferation findings, we asked whether catalase, acting as an exogenous H_2O_2 scavenger, would mimic the effects of Duox1deficiency, thereby leading to enhanced proliferation of WT CD19^{+} B cells. Cultivation with catalase in the media for 72 h led to increased actual numbers of proliferating WT cells either following stimulation with anti-IgM F(ab')$_2$ alone or with anti-IgM F(ab')$_2$ and IL-4 together (Figure 5). Meanwhile, PI^{+} cell numbers were unaffected by addition of catalase to these proliferating WT CD19^{+} B cell populations.

We investigated whether B cell immunoglobulin production is influenced by Duox1, by comparing both *in vitro* and *in vivo* production of each Ig isotype (Figure 6 and

Supplementary Fig. 3). Several stimulants tested under *in vitro* conditions induced production of IgM, IgG1, IgG2a, IgG2b, IgG3 and IgA by $CD19^+$ B cells, but their levels were comparable in WT and Duox1-deficient cell cultures (Figure 6). Nox2-deficient cells showed lower production of IgM, IgG1, IgG2a, IgG2b and IgG3 following several kinds of co-stimulation in comparison with WT cells.

We subsequently examined production levels of antigen-specific antibody *in vivo* by immunization with TI antigen or TD antigen (Supplementary Fig. 3a–c). In order to compare early-phase Ig production responses between WT and $Duox1^{-/-}$ mice, we detected serum IgM level in immunized mice with TI antigen. Duox1 deficiency showed comparable levels of serum IgM at 8 days post-immunization with TI antigen in comparison to its levels in WT mice (Supplementary Fig. 3a). To focus on later responses of Ig isotype production, serum IgM and IgG1 levels in WT and $Duox1^{-/-}$ mice were monitored at 14 days post-immunization with TD antigens. Both mouse strains did not exhibit any differences in IgM and IgG1 production levels at 14 days post-immunization by TD antigen (Supplementary Fig. 3c). Meanwhile, Nox2-deficient mice showed comparable levels of serum IgM with those of WT or $Duox1^{-/-}$ mice at 7 days post-immunization with TI antigen (Supplementary Fig. 3b).

We investigated proliferation of B cells within GCs in the spleen from immunized mice by immunohistological evaluation of several markers (Figure 7 and Table 1). At 8 days post-immunization with TI antigen (NP-LPS), histological examination of Duox1-deficient spleens revealed greatly enhanced signals of the B cell proliferation marker Ki67 within follicular regions identified by the B cell lineage marker Pax5 in comparison to WT and Nox2 mutant mice (Figure 7a and Table 1). Increased numbers of GCs were also observed, along with the increased GC size and reactivity detected by GC marker PNA positivity, in the spleens from $Duox1^{-/-}$ mice relative to the other strains following TI immunization (Figure 7b). In contrast, we detected no remarkable immunohistochemical staining pattern differences among the three mouse strains following immunization with TD antigen (NP-KLH, 14 days; Supplementary Fig. 3d). Together the above findings suggest Duox1-derived H_2O_2 plays some role in restricting splenic $CD19^+$ B cell proliferation, but does not affect Ig isotype production.

Discussion

Deliberate and robust production of ROS by phagocytic blood cells has long been recognized as a unique feature of these cells referred to as the “respiratory burst”, which is activated by phagocytic stimuli for oxidant-based microbial killing (26, 27). This activity is attributed to a multi-component Nox2-based NADPH oxidase in phagocytes, although this enzyme is also detected in B lymphocytes. Studies on the role of ROS in primary B cells have revealed that Nox2-derived $O_2{\cdot}^-$ influences B cell functions, such as altering production of Ig isotypes from several B cell subsets in mice and humans (8, 10, 11). Our current studies using both *in vitro* and *in vivo* approaches confirmed a role for Nox2 in the early phase of ROS generation post-stimulation, and then focused on another T_H2 cytokine-inducible ROS generator, Duox1, to explore its capacity for H_2O_2 production and

downstream functional consequences in comparison with Nox2-derived $O_2\cdot^-$ in primary B cells.

Splenic $CD19^+$ B cells lacking Duox1 showed normal basal expression of Nox1, Nox2, Nox3, Nox4 and Duox2 transcripts under non-stimulated healthy conditions. Early phase H_2O_2 levels detected in the vicinity of stimulated BCR by OxyBURST-conjugated anti-IgM $F(ab')_2$ were comparable between WT and $Duox1^{-/-}$ $CD19^+$ cells, whereas Nox2-deficient cells showed a remarkable reduction of detectable H_2O_2 in our experiments. Nox2 is an abundant NADPH oxidase in peripheral and BM-derived Ig-expressing B cells that produces $O_2\cdot^-$ through mitogenic stimulation of human B cells (5). In mouse splenic resting B cells, the Nox2 transcript is the predominant NADPH oxidase detected in either stimulated or unstimulated cells; $O_2\cdot^-$ produced following BCR stimulation is converted into H_2O_2, which can be detected in the vicinity of BCR with OxyBURST Green conjugated to anti-IgM $F(ab')_2$ (Fig. 1c and ref. 11). These findings indicate that H_2O_2 localized within the vicinity of BCR is mainly supplied by Nox2-derived superoxide intermediate in the early phase of BCR stimulation, rather than Duox1-derived H_2O_2. Previous studies by Singh, *et al*, using RNA silencing methodology in A20 lymphoma cells suggested Duox1 is a source of early-phase ROS elicited by anti-IgG $F(ab')_2$ stimulation alone (15), although effects of Nox2 silencing in this cell line were not examined.

We showed that co-stimulation with anti-IgM $F(ab')_2$ and IL-4 enhanced expression of Duox1 among all the NADPH oxidase gene family members surveyed in splenic $CD19^+$ B cells. In human keratinocytes and airway epithelial cells, treatment with IL-4 induces upregulation of Duox1 production concomitant with enhanced H_2O_2 generation in these cells (16–20). Our studies found that primary $CD19^+$ B lymphocytes exhibit enhanced Duox1 expression and H_2O_2 production 24 h following co-stimulation with IL-4 (Fig. 2a, Supplementary Fig. 1), whereas H_2O_2 production was greatly diminished in Duox1-deficient cells. whereas The H_2O_2 levels detected in Nox2-deficient cells were comparable with that in WT cells, even though intracellular $O_2\cdot^-$ production was attenuated in these mutant cells (Fig. 2b). These results suggest that Duox1-derived H_2O_2 release at 24 h by BCR-stimulated cells under the influence of IL-4 co-stimulation becomes predominant relative to the H_2O_2 converted from Nox2-derived $O_2\cdot^-$. In other experiments, we found that IL-13 does not induce enhanced expression of Duox1 or H_2O_2 production in $CD19^+$ B cells (Supplementary Fig. 1), consistent with observations that mouse B cells express little or no IL-13Rα1, but high levels of a decoy receptor, IL-13Rα2, which lacks a signaling domain (28–31).

The observation of enhanced proliferation of B cells that lack Duox1-derived H_2O_2 raises a question because PTPases such as SHP-1 are thought to inhibit BCR signaling. Negative regulation of SHP-1 by Duox1-derived H_2O_2 could potentially enhance B cell activity, including proliferation through oxidation of SHP-1, as suggested by the findings in A20 lymphoma cells (15). However, their study never examined the prolonged effects of Duox1 silencing on cell proliferation. Our observations did not support a role for Duox1 in early-phase ROS generation or proximal BCR signaling, and the loss of H_2O_2 due to Duox1 knockout increases proliferation of splenic $CD19^+$ B cells. In our *in vivo* approaches using whole immunized mice, Duox1 deficiency indeed leads to enhanced B cell proliferation within germinal centers in spleens of whole immunized mice, further supporting our

proposal that Duox1 restricts B cell proliferation. Another study using CD19-cre-conditional SHP-$1^{-/-}$ mice demonstrated that Ca^{2+} influx induced by BCR stimulation with anti-IgM $F(ab')_2$ is downregulated by SHP-1 in the B-1a cells, whereas the Ca^{2+} response is not influenced at all by the PTPase in B-2 cells among total $CD19^+$ splenic cells (32). These finding indicates that not all primary B cell subsets are regulated by SHP-1. Thus, the issue of whether the popularly held SHP-1 oxidation-based paradigm applies to BCR signaling remains debatable, particularly in late-phase responses.

In our experiments with primary $CD19^+$ B cells co-stimulated with anti-IgM $F(ab')_2$ and IL-4 for 24 h, the absence of Duox1 did not affect BLNK gene expression; this led instead to upregulation of another adaptor molecule, B-cell adapter for PI3K (BCAP). BCAP mediates BCR signaling via Src family kinases by phosphorylating itself and serving as an intermediary in the downstream Akt pathway, thereby positively regulating proliferative activity of B cells (33, 34). In the current study, BCAP expression was increased by Duox1 deficiency, but does not appear to influence the phosphorylation and production of Akt (Fig 3c–e). Nonetheless, Duox1-deficient $CD19^+$ B cells showed enhanced proliferation by BCR stimulation with anti-IgM $F(ab')_2$ or additional IL-4 co-stimulation, which upregulates Duox1 expression in WT cells. Thus, it appears that Duox1-derived H_2O_2 restricts proliferative activity independent of the Akt pathway. We further showed the increased proliferation observed with Duox1-deficient cells could be mimicked with WT cells by scavenging H_2O_2 with catalase (Fig. 5). Catalase is naturally deployed in intracellular peroxisomes (35) and this enzyme converts H_2O_2 into less-reactive stable substances, H_2O and oxygen, to regulate excessive cell signaling (36) as well as preventing cytotoxic damage (37). Supplementation with catalase promotes decomposition of Duox1-derived H_2O_2, which thereby diminishes the suppressive effects of Duox1 on proliferation of $CD19^+$ B cells, further supporting our hypothesis that Duox1 plays a negative role in proliferation.

Enhanced proliferative activity of Nox2 ($gp91^{phox}$)-deficient $CD19^+$ cells co-stimulated with anti-IgM $F(ab')_2$ and IL-4 was also observed in our experiments, albeit to a lesser extent than in Duox$1^{-/-}$ cells. Similar effects of enhanced proliferation associated with $gp91^{phox}$ deficiency in total splenic B cells were reported previously (10). Here, Nox2-derived $O_2{\cdot}^-$ production following BCR stimulation appears to upregulate $p27^{kip1}$, which acts as a brake on the G_0 to G_1 transition of the cell cycle to promote B cell proliferation. Thus, the enhanced proliferation of Nox2-deficient ($gp91^{phox-/-}$) $CD19^+$ B cells that we observed likely reflects relief of inhibitory effects of $p27^{kip1}$. On the other hand, it was reported that resting splenic B cells from Neutrophil cytosolic factor 1 ($Ncf1/p47^{phox}$) mutant mice that are functionally Nox2 deficient show normal proliferative responses to mitogenic stimuli (11). Neutrophils from CGD patients with $p47^{phox}$ deficiency show some residual NOX2 activity (38), which may explain the discrepancy in proliferation responses between Ncf1- and Nox2-deficient B cells.

Duox1 deficiency also significantly increased RGS16 expression in $CD19^+$ B cells following co-stimulation. Upregulation of RGS16 expression was observed in human primary keratinocytes in which Duox1 was silenced by RNA interference, suggesting that RGS16 expression is negatively-regulated by Duox1-derived H_2O_2 (20). It appears that RGS16 retains B cell within GCs to suppress B cell migration induced by CXCR4 chemokine (39,

40). Our *in vivo* TI antigen immune challenge experiments detected increased B-cell proliferation in GC of spleens of Duox1$^{-/-}$ mice. Therefore, enhanced RGS16 expression caused in the absence of Duox1 could favor localization of CD19^{+} B cells within GCs to further induce robust proliferative activity.

Typically, TI immunization induces rapid, but transient, GC formation, as class-switching and somatic hypermutation does not occur without T cell help, such that basal production of antigen-specific IgM is elevated through expansion of single or limited numbers of germline-derived, low-affinity antibody B cell clones (41, 42). Our study showed that Duox1 deficiency in CD19^{+} B cells resulted in normal *in vitro* production of 6 Ig isotypes following stimulation with anti-IgM F(ab')$_2$ or anti-CD40 in the presence or absence of IL-4 (Figure 6). Likewise, Duox1-deficient mice showed comparable serum IgM production relative to WT mice following a single immunization with the TI antigen NP-LPS (Supplementary Fig. 3a, b). The absence of Duox1 in mice also did not significantly influence serum IgM and IgG isotype production following single TD-antigen immunizations (Supplementary Fig. 3c). Although Duox1-derived H_2O_2 does not appear to play a critical role in regulation of Ig isotype production in response to single TI or TD antigen imunizations, our observations on CD19^{+} B cell proliferation *in vitro* and *in vivo* suggest Duox1 could have a role in restricting clonal B cell expansion in response to certain antigenic stimuli. TI immunization not only induces transient GC formation (41, 42 and Fig. 7a), but also generates and maintains long-lived plasma cells in both spleen and BM (43). Long-term IgM-dependent protection against specific pathogens that induce TI-type immunity, such as *Streptococcus pneumoniae* and *Entamoeba muris*, has been attributed to TI-induced memory B and long-lived plasma cells (43, 44). Thus, Duox1 may influence immune defense reactions by regulating B-cell proliferation during repeated or sustained microbial infections, particularly by specific pathogens that evade TD immune responses, and may affect the generation of long-lived plasma cells that contribute to host immune homeostasis.

On the other hand, Nox2 deficiency led to decreases of IgM, IgG1, IgG2a and IgG2b production in CD19^{+} B cells following stimulation with anti-IgM F(ab')$_2$ in the presence of IL-4 *in vitro*. In contrast, specific IgM levels in sera from Nox2$^{-/-}$ mice were not lower than that of WT post-immunization with TI antigen (Supplementary Fig. 3b). Several studies reported that immunization of Nox2$^{-/-}$ animal models with TD- or TI-antigen enhances production of antigen-specific IgM and IgG isotypes *in vivo* (10, 11). How Nox2 deficiency causes such disparate effects on Ig production *in vitro versus in vivo* is not entirely clear. We did observe significant increases in PI^{+} events in Nox2-deficient CD19^{+} B cells in culture following BCR stimulation, explaining how the lack of Nox2 could adversely affect production of several Ig isotype *in vitro*. In several non-phagocytic cell types, such as pancreatic cancer, vascular endothelial cells, or cardiomyocytes, suppression of Nox2 attenuates $O_2\cdot^{-}$ production and causes decreased cell viability (45–47). Silencing of Nox2 activates the caspase pathway in vascular endothelial cells, suggesting Nox2 serves anti-apoptotic or pro-survival roles in non-phagocytic cells (45). Furthermore, Nox2 or Ncf1 knockout cardiomyocytes showed decreased viability (46). A Nox2-induced cell survival mechanism is supported by our current findings in the primary CD19^{+} B cells. In contrast, loss of H_2O_2 with Duox1 deficiency did not increase the proportion of PI^{+} cells among CD19^{+} B cells relative to WT cells treated under the same proliferating conditions.

Moreover, supplementation with the H_2O_2 scavenger catalase during cultivation with stimuli caused enhanced cell proliferation but had no effects on PI^+ events in WT $CD19^+$ B cells. These observations suggest that Duox1-derived H_2O_2, unlike Nox2-derived $O_2\cdot^-$, does not influence survival or death responses of primary $CD19^+$ B cells.

Our current studies focused primarily on murine splenic $CD19^+$ B cells, which would encompass most B cell subsets in the spleen (48, 49), to elucidate roles of Duox1-derived H_2O_2 in primary B cells. Using this approach, we found that Duox1 under the influence of IL-4 negatively regulates stimulus-induced proliferation through production of H_2O_2. Consistent with these observations, we found that scavenging H_2O_2 with catalase *in vitro* supports the expansion of WT $CD19^+$ B cell without influencing cell viability, suggesting a potential means for development of B cell modifications *ex vivo* for clinical applications. Other experiments in whole animals immunized with TI antigen confirmed that the anti-proliferative effects of Duox1 are also manifested *in vivo*, where we observed rapid increases in the size and number of GCs in spleens of $Duox1^{-/-}$ mice; in contrast, we observed no effects of Duox1 deficiency on GC development or immune responses to TD antigen immunization. Our findings suggest that Duox1 may impact B cell proliferation in the reaction to microbial infections, particularly by pathogens that induce TI responses. Thus, future studies should investigate whether Duox1 regulates long-term humoral immune defense against such pathogens by affecting the expansion of B cell populations in sites beyond splenic GCs or the generation and longevity of long-lived plasma cells.

Supplementary Material

Refer to Web version on PubMed Central for supplementary material.

Acknowledgements

We thank Dr. Miklos Geiszt (Semmelweis University, Hungary) for providing the Duox1 knockout mice. We also thank members of the NIAID Research Technologies Branch for assistance with flow cytometry and Donna Butcher (NCI-Frederick) and Jawara Allen for providing immuno-histochemistry technical support and advice.

This work was supported by the Intramural Research Program of the National Institute of Allergy and Infectious Diseases, NIH, ZIA AI001060-11.

References

1. Kurosaki T, Shinohara H, and Baba Y 2010 B cell signaling and fate decision. Annu. Rev. Immunol 28 21–55. [PubMed: 19827951]
2. Paus D, Phan TG, Chan TD, Gardam S, Basten A and Brink R 2006 Antigen recognition strength regulates the choice between extrafollicular plasma cell and germinal center B cell differentiation. J. Exp. Med 203:1081–1091. [PubMed: 16606676]
3. Reth M, and Brummer T 2004 Feedback regulation of lymphocyte signalling. Nat. Rev. Immunol 4: 269–277. [PubMed: 15057785]
4. Smith KG, Tarlinton DM, Doody GM, Hibbs ML and Fearon DT 1998 Inhibition of the B cell by CD22: a requirement for Lyn. J. Exp. Med 187: 807–811. [PubMed: 9480991]
5. Kobayashi S, Imajyo-Ohmi S, Nakamura M, and Kanegasaki S 1990 Occurrence of cytochrome b_{558} in B-cell lineage of human lymphocytes. Blood 75: 458–461. [PubMed: 2153037]
6. Kovac I, Horvath M, Lanyi A, Petheo GL, and Geiszt M 2015, Reactive oxygen species-mediated bacterial killing by B lymphocytes. J. Leuk. Biol 97: 1133–1137.

7. Bleesing JJ, Souto-Carneiro MM, Savage WJ, Brown MR, Martinez C, Yavuz S, Brenner S, Siegel RM, Horwitz ME, Lipsky PE, Malech HL, and Fleisher TA 2006 Patients with chronic granulomatous disease have a reduced peripheral blood memory B cell compartment. J. Immunol 176: 7096–7103. [PubMed: 16709872]
8. Moir S, Ravin SSD, Santich BH, Kim JY, Posada JG, Ho J, Buckner CM, Wang W, Kardava L, Garofalo M, Marciano BE, Manischewitz J, King LR, Khurana S, Chun TW, Golding H, Fauci AS, and Malech HL 2012 Humans with chronic granulomatous disease maintain humoral immunologic memory despite low frequencies of circulating memory B cells. Blood 120: 4850–4858. [PubMed: 23074274]
9. Cotugno N, Finocchi A, Cagigi A, Di Matteo G, Chiriaco M, Di Cesare S, Rossi P, Aiuti A, Palma P, and Douagi I (2015). Defective B-cell proliferation and maintenance of long-term memory in patients with chronic granulomatous disease. J. Allergy Clin. Immunol135: 753–761. [PubMed: 25175493]
10. Richards SM, and Clark EA 2009 BCR-induced superoxide negatively regulates B-cell proliferation and T-cell-independent type 2Ab responses. Eur. J. Immunol 39: 3395–3403. [PubMed: 19877015]
11. Wheeler ML, and Defranco AL 2012 Prolonged production of Reactive Oxygen Species in response to B cell receptor stimulation promotes B cell activation and proliferation. J. Immunol 189: 4405–4416. [PubMed: 23024271]
12. Morand S, Ueyama T, Tsujibe S, Saito N, Korzeniowska A, and Leto TL, 2009 DUOX maturation factors form cell surface complexes with DUOX affecting the specificity of reactive oxygen species generation. FASEB J. 11: 2607–2619.
13. Rada B and Leto TL 2008 Oxidative innate immune defenses by NOX/DUOX family NADPH oxidases. Contrib. Microbiol 15: 164–187. [PubMed: 18511861]
14. Kwon J, Shatynski KE, Chen H, Morand S, Deken X, Miot F, Leto TL, and Williams MS 2010 The nonphagocytic NADPH oxidase DUOX1 mediates a positive feedback loop during T cell receptor signaling. Immunology 3;3(133):ra59. doi: 10.1126/scisignal.2000976.
15. Singh DK, Kumar D, Siddiqui Z, Basu SK, Kumar V and Rao KVS 2005 The strength of receptor signaling is centrally controlled through a cooerative loop between Ca^{2+} and an oxidant signal. Cell 121: 281–293. [PubMed: 15851034]
16. Harper RW, Xu C, Eiserich JP, Chen Y, Kao CY, Thai P, Setiadi H, and Wu R 2005 Differential regulation of dual NADPH oxidases/peroxidases, DUOX1 and DUOX2, by Th1 and Th2 cytokines in the respiratory tract epithelium. FEBS Lett. 579: 4911–4917. [PubMed: 16111680]
17. Rada B, Lekstrom KJ, Damian S, Dupuy C, and Leto TL 2008, The Pseudomonas toxin pyocyanin inhibits the dual oxidase-based antimicrobial system as it imposes oxidative stress on airway epithelial cells. J. Immunol 181: 4883–4893. [PubMed: 18802092]
18. Hristova M, Habibovic A, Veith C, Janssen-Heininger YMW, Dixon AE, Geiszt M, and van der Vliet A 2015 Airway epithelial dual oxidase 1 mediates allergen-induced IL-33 secretion aand activation of type 2 immune responses. J. Allergy Clin. Immunol 137: 1545–1556.e11. doi: 10.1016/j.jaci. [PubMed: 26597162]
19. Chang S, Linderholm A, Franzi L, Kenyon N, Grasberger H, and Harper RW 2013 Dual oxidase regulates neutrophil recruitment in allergic airways. Free Rad. Biol. Med 65: 38–46. [PubMed: 23770197]
20. Hirakawa S, Saito R, Ohara H, Okuyama R, and Aiba S 2011 Dual Oxidase 1 induced by Th2 cytokines promotes STAT6 phosphorylation via oxidative inactivation of protein tyrosine phosphatase 1B in human epidermal keratinocytes. J. Immunol 186: 4762–4770. [PubMed: 21411736]
21. Zambrowicz BP, Friedrich GA, Buxton EC, Lilleberg SL, Person C and Sands AT 1998 Disruption and sequence identification of 2,000 genes in mouse embryonic stem cells. Nature 392: 608–611. [PubMed: 9560157]
22. Donkó A, Ruisanchez E, Orient A, Enyedi B, Kapui R, Péterfi Z, de Deken X, Benyó Z and Geiszt M 2010 Urothelial cells produce hydrogen peroxide through the activation of DUOX1. Free Radic. Biol. Med 49: 2040–2048. [PubMed: 21146788]

23. Allman D, Lindsley C, DeMush W, Rudd K, Shinton SA, and Hardy RR 2001 Resolution of three nonproliferative immature splenic B cell subsets reveals multiple selection points during peripheral B cell maturation. J. Immunol 167: 6834–6840. [PubMed: 11739500]
24. Cappasso M, Bhamrah MK, Henley T, Boud RS, Langlais C, Cain K, Dinsdale D, Pulford K, Khan M, Musset B, Cherny V, Morgan D, Gascoyne RD, Vigorite E, DeCoursey TE, MacLennan ICM and Dyer MJS 2010 HVCN1 modulates BCR signal strength via regulation of BCR-dependent generation of reactive oxygen species. Nat. Immunol 11: 265–272. [PubMed: 20139987]
25. Qi CF., Hori M, Coleman AE, Torrey TA, Taddesse-Heath L, Ye BH, Chattopadhyay SK,, Hartley JW, Morse HC, 3rd. 2000 Genomic organisation and expression of BCL6 in murine B-cell lymphomas. Leuk. Res 24: 719–732. [PubMed: 10936424]
26. Morel F, Doussiere J, and Vignais PV 1991 The superoxide-generating oxidase of phagocytic cells. Physiological, molecular and pathological aspects. Eur. J. Biochem 201: 523–546. [PubMed: 1657601]
27. Bellavite P 1988 The superoxide-forming enzymatic system of phagocytes. Free. Radic. Bio. Med 4: 225–261. [PubMed: 2834275]
28. Wills-Karp M and Finkelman FD 2008 Untangling the complex web of IL-4- and IL-13-mediated signaling pathways. Sci. Signal 1:pe55. doi: 10.1126/scisignal.1.51.pe55. [PubMed: 19109238]
29. Donaldson DD, Whitters MJ, Fitz LJ, Neben TY, Finnerty H, Henderson SL, O'Hara RM, Jr., Beier DR, Turner KJ, Wood CR, and Collins M 1998 The murine IL-13 receptor alpha 2: molecular cloning, characterization, and comparison with murine IL-13 receptor alpha 1. J. Immunol 161: 2317–2324. [PubMed: 9725226]
30. de Vries JE 1998 The role of IL-13 and its receptor in allergy and inflammatory responses. J. Allergy Clin. Immunol 102: 165–169. [PubMed: 9723655]
31. Andrews R, Rosa L, Daines M, and Khurana-Hershey G 2001 Reconstitution of a functional human type II IL-4/IL-13 receptor in mouse B cells: demonstration of species specificity. J. Immunol 166: 1716–1722. [PubMed: 11160216]
32. Pao LI, Lam KP, Henderson JM, Kutok JL, Alimzhanov M, Nitschke L, Thomas ML, Neel BG, and Rajewsky K 2007 B cell-specific deletion of protein-tyrosine phosphatase Shp1 promotes B-1a cell development and causes systemic autoimmunity. Immunity 27: 35–48. [PubMed: 17600736]
33. Okada T, Maeda A, Iwamatsu A, Gotoh K and Kurosaki T 2000 BCAP: the tyrosine kinase substrate that connects B cell receptor to phosphoinositide 3-kinase activation. Immunity 13: 817–827. [PubMed: 11163197]
34. Yamazaki T and Kurosaki T 2003 Contribution of BCAP to maintenance of mature B cells through c-Rel. Nat. Immunol 4: 780–786. [PubMed: 12833156]
35. Schrader M, and Fahimi HD 2006 Peroxisomes and oxidative stress. Biochim. Biophys. Acta 1763: 1755–1766. [PubMed: 17034877]
36. Yano S and Yano N 2002 Regulation of catalase enzyme activity by cell signaling molecules. Mol. Cell Biochem. 240: 119–130. [PubMed: 12487379]
37. Siraki AG, Pourahmad J, Chan TS, Khan S and O'Brien PJ 2002 Endogenous and endobiotic induced reactive oxygen species formation by isolated hepatocytes. Free Radic. Biol. Med 32: 2–10. [PubMed: 11755311]
38. Kuhns DB, Alvord WG, Heller T, Feld JJ, Pike KM, Marciano BE, Uzel G, Deravin SS, Priel DA, Soule BP, Zarember KA, Holland SM, and Gallin JI 2010 Residual NADPH oxidase survival in chronic granulomatous disease. N. Engl. J. Med 363: 2600–2610. [PubMed: 21190454]
39. Hsu HC, Yang P, Wang J., Wu Q., Myers R., Chen J., Yi J., Guentert T., Tousson A., Stanus A,L., Le T,V., Lorenz R,G., Xu H., Kolls J,K., Carter R,H., Chaplin D,D., Williams R,W., and Mountz J,D. 2008 Interleukin 17-producing T helper cells and interleukin 17 orchestrate autoreactive germinal center development in autoimmune BXD2 mice. Nat. Immunol 9: 166–175. [PubMed: 18157131]
40. Xie S, Li J., Wang J,H., Wu Q., Yang P., Hsu H,C., Smythies L,E., and Mountz J,D. 2010 IL-17 activates the canonical NF-kappaB signaling pathway in autoimmune B cells of BXD2 mice to upregulate the expression of regulators of G-protein signaling 16. J. Immunol 184: 2289–2296. [PubMed: 20139273]

41. Lentz VM, and Manser T 2001 Cutting edge: Germinal centers can be induced in the absence of T cells. J. Immunol 167: 15–20. [PubMed: 11418626]

42. Toellner KM, Jenkinson WE, Taylor DR, Khan M, Sze DMY, Sansom DM, Vinuesa CG, and MacLennan CM 2002 Low-level hypermutation in T cell-independent germinal centers compared with high mutation rates associated with T cell-dependent germinal centers. J. Exp. Med 195: 383–389. [PubMed: 11828014]

43. Bortnick A, Chernova I, Quinn WJ, Mugnier M, Cancro MP, and Allman D 2012 Long-lived bone marow plasma cells are induced early in response to T cell-independent or T cell-dependent antigens. J. Immunol 188: 5389–5396. [PubMed: 22529295]

44. Obukhanych TV, and Nussenzweig MC 2006 T-independent type II immune responses generate memory B cells. J. Exp. Med 203: 305–310. [PubMed: 16476769]

45. Peshavariya H, Dusting GJ, Jiang F, Halmos LR, Sobey CG, Drummond GR and Selemidis S 2009 NADPH oxidase isoform selective regulation of endothelial cell proliferation and survival. Naunyn. Schmiedebergs. Arch. Pharmacol 380: 193–204. [PubMed: 19337723]

46. Du J, Nelson ES, Simons AL, Olney KE, Moser JC, Schrock HE, Wagner BA, Buettner GR, Smith BJ, Teoh ML, Tsao MS and Cullen JJ 2013 Regulation of pancreatic cancer growth by superoxide. Mol. Carcinog 52: 555–567. [PubMed: 22392697]

47. Rosc-Schlüter BI, Häuselmann SP, Lorenz V, Mochizuki M, Facciotti F, Pfister O, Kuster GM 2012 NOX2-derived reactive oxygen species are crucial for CD29-induced prosurvival signaling in cardiomyocytes. Cardiovasc. Res 93: 454–462. [PubMed: 22198504]

48. Hardy RR, and Shinton SA 2004 Characterization of B lymphopoiesis in mouse bone marrow and spleen. Methods Mol. Biol 271: 1–24. [PubMed: 15146109]

49. Vugmeyster Y, Howell K, Bakshi A, Flores C, Hwang O, and McKeever K 2004 B-cell subsets in blood and lymphoid organs in Macaca fascicularis. Cytometry A. 61: 69–75. [PubMed: 15351991]

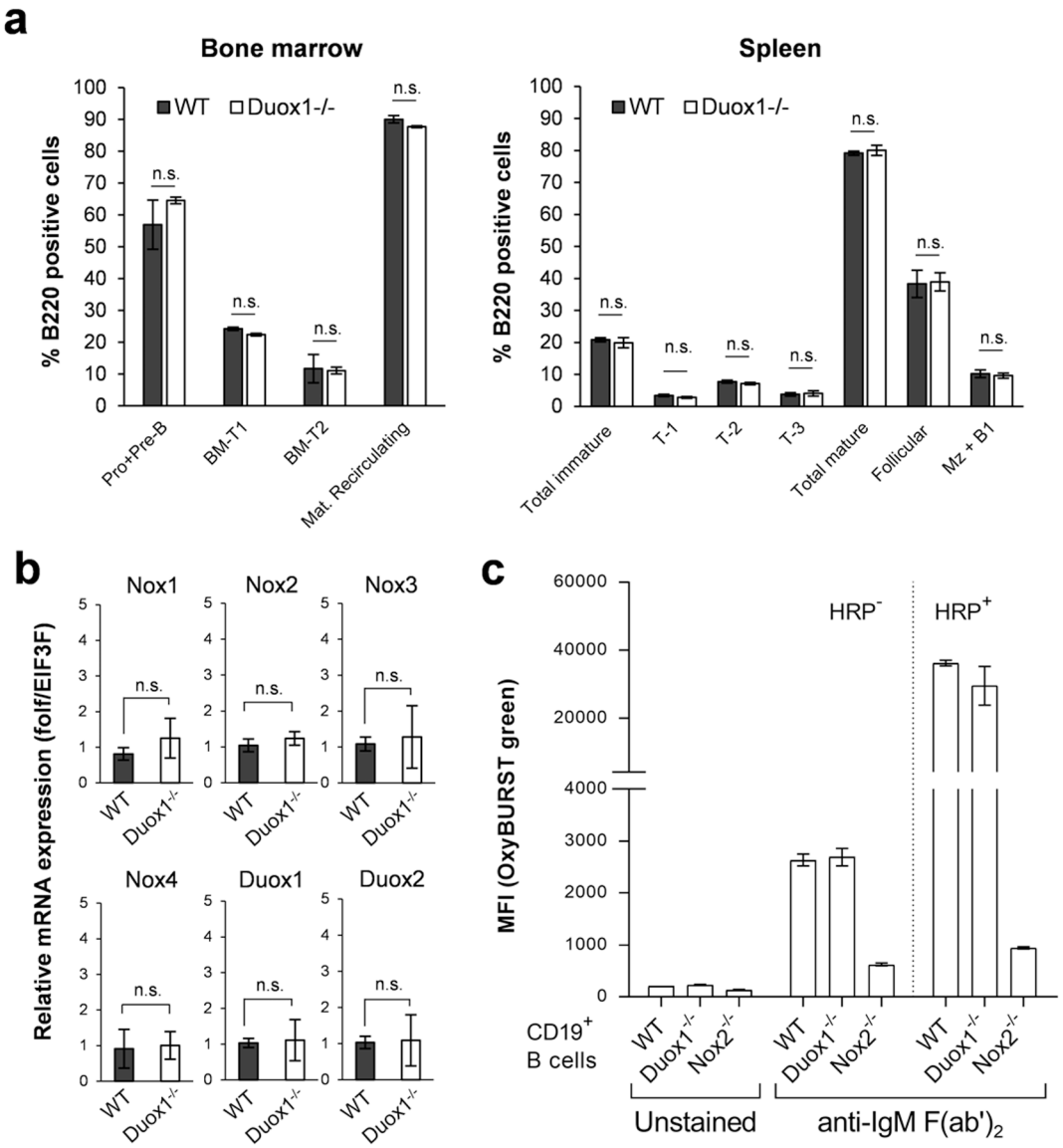

Figure 1.

Duox1 deficiency does not alter B cell homeostasis or early oxidative responses to BCR stimulation. (a) Development and maturation of each B cell subset in bone marrow and spleen. Bone marrow cells and splenocytes collected from 8–12 week-old mice were stained with fluorescence-conjugated anti-CD23, anti-IgM, anti-CD93 and anti-B220, and the distribution of each B cells subset was analyzed by flow cytometry. Frequencies of each B cell subtypes in bone marrow and spleen are shown as percentages of $B220^+$ cells from WT and $Duox1^{-/-}$ mice. Data are expressed as mean ±s.e. of results from 4–6 mice of each strain. n.s., not significant difference (unpaired Student's *t*-test). (b) Gene expression patterns of Nox/Duox family members in freshly isolated non-stimulated $CD19^+$ B cells. The expression of each gene was normalized to the levels of eukaryotic translation initiation factor 3, subunit F (EIF3F) mRNA. Duox1 mRNAs from $Duox1^{-/-}$ mice were detected as a frame-shifted transcript (22). Data are expressed as mean ±s.e. of results from three mice

(WT: n=3, Duox1$^{-/-}$: n=3). n.s., nonsignificant differences (unpaired Student's t-test). (c) Early phase ROS production by splenic CD19^{+} B cells following BCR stimulation in the presence or absence of HRP. H_2O_2 was detected in the vicinity of BCR with DCFDA-conjugated anti-IgM F(ab')$_2$ by flow cytometry. Data are shown as mean fluorescence intensity (MFI) of FITC channel fluorescence from 2 mice in each strain, WT, Duox1$^{-/-}$ or Nox2$^{-/-}$.

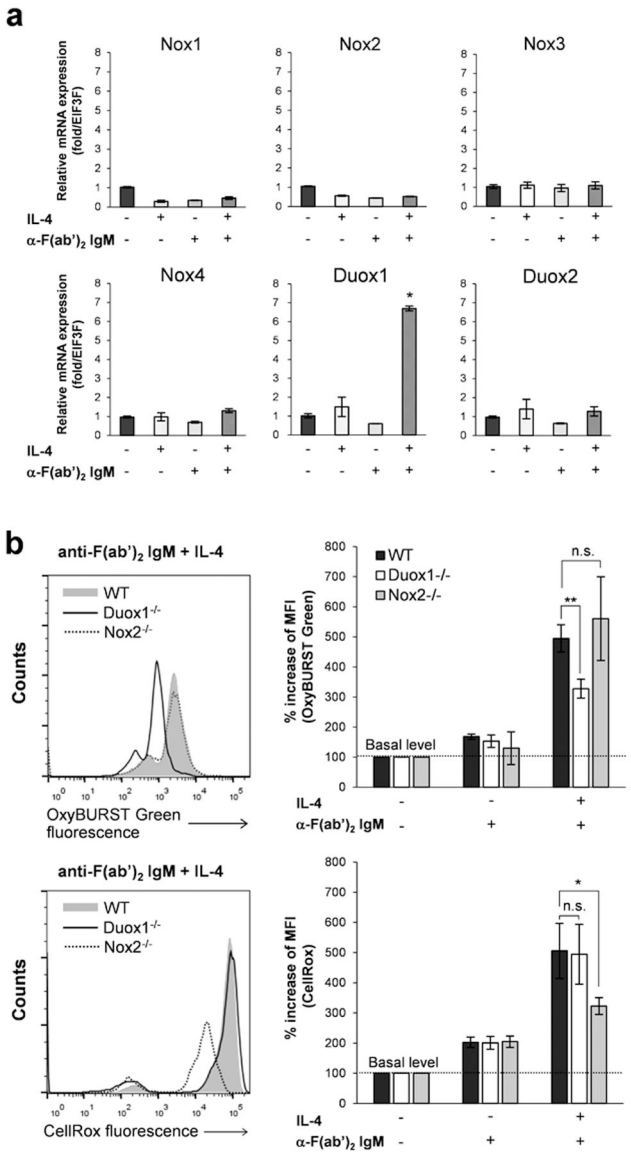

Figure 2.

IL-4 induces Duox1-dependent H_2O_2 production by $CD19^+$ B cells (a) Relative expression of Nox/Duox genes in $CD19^+$ B cells stimulated for 24 h by IL-4 (20 ng/ml), anti-IgM $F(ab')_2$ (5 μg/ml) or a combination of both. Expression of each NADPH oxidase was examined by RT-qPCR and normalized to unstimulated cell levels relative to EIF3F mRNA. Data are expressed as mean ±s.e. of results from four WT mice. $*p < 0.05$ (paired Student *t*-test). (b) ROS production in 24-h stimulated $CD19^+$ B cells from spleens of WT, Duox1-deficient and Nox2-deficient mice. Representative histograms of ROS detection in stimulated $CD19^+$ B cells by cell surface-conjugated OxyBURST Green-SE fluorescence (upper left panel) or intracellular CellRox fluorescence (lower left panel). Cells were costimulated by anti-IgM $F(ab')_2$ and IL-4 for 24 h, collected and labeled or loaded with both dye reagents in the presence of HRP, and then analyzed by flow cytometry. Right

panels summarize data on percent increase of mean fluorescence intensities (MFI) ±s.e. (WT: n=8, Duox1$^{-/-}$: n=5, and Nox2$^{-/-}$: n=3). *$p < 0.05$ (unpaired Student t-test).

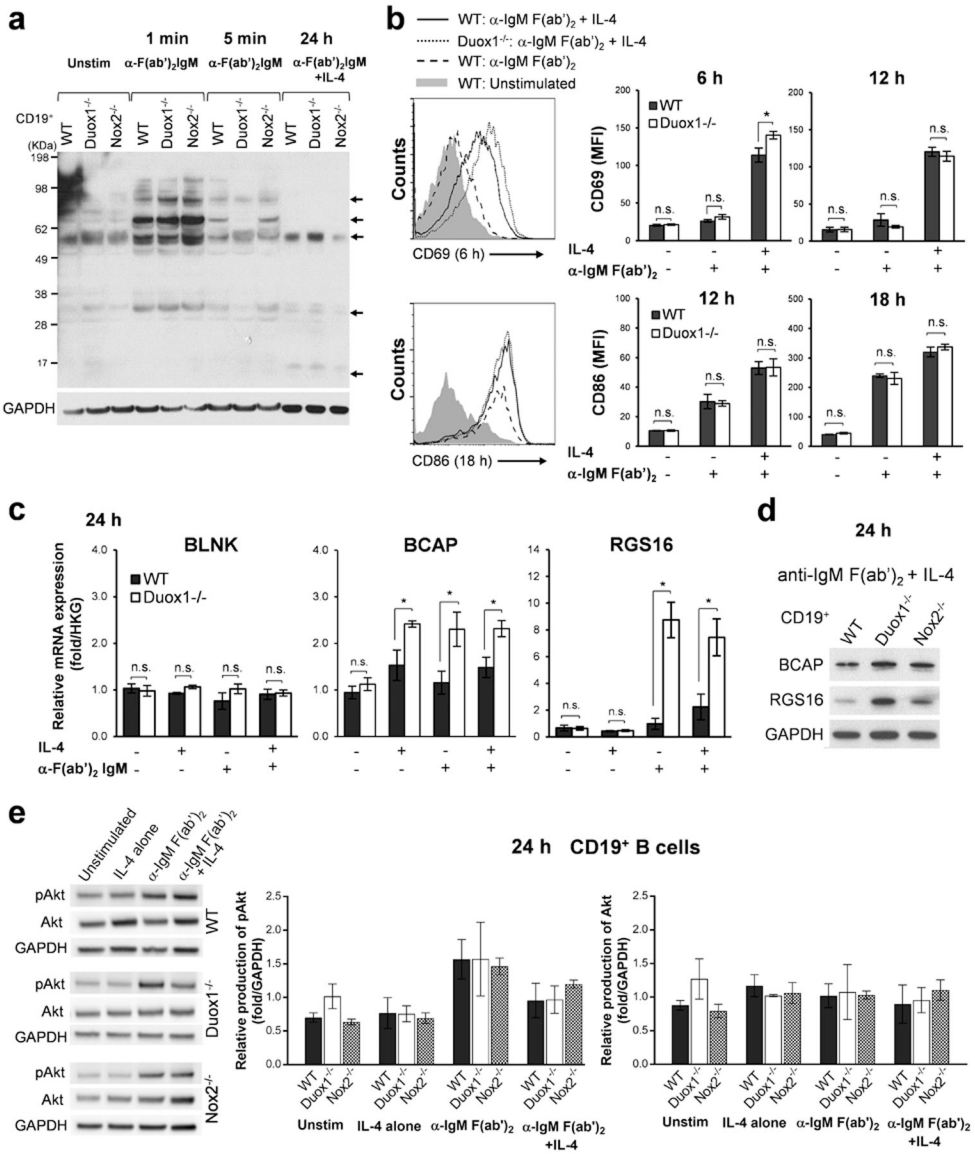

Figure 3.

Duox1 affects expression of B cell activation markers and BCR signal mediators (a) Total phosphotyrosine (p-Tyr) immunoblot (fingerprint) analysis of unstimulated or stimulated splenic CD19$^+$ B cells from WT, Nox2$^{-/-}$ and Duox1$^{-/-}$ mice. Differential phosphorylation patterns between WT and mutant CD19$^+$ B cells are indicated by arrows on the right. (b) Cell surface expression of CD69 and CD86 in stimulated CD19$^+$ B cells. (Left) a representative histogram showing expression at 6 or 18 h post-stimulation which was analyzed by flow cytometry comparing MFI between WT and Duox1$^{-/-}$ CD19$^+$ B cells (Right). Data are shown as MFI ±s.e of results from four mice each, at multiple time-points post stimulation. n.s., not significant difference *$p < 0.05$ (paired Student t-test). (c) Expression of BCR signaling mediators. Relative expression after 24 h stimulation was normalized to EIF3F and compared between WT and Duox1$^{-/-}$ CD19$^+$ B cells. Data are expressed as mean ±s.e. (WT: n=5, Duox1$^{-/-}$: n=6). *$p < 0.05$ (paired Student t-test). (d)

Immunoblotting of BCAP and RGS16 in $CD19^+$ B cells after 24 h stimulation with anti-IgM $F(ab')_2$ and IL-4. (e) Akt protein production and phosphorylation. (Left) Representative immunoblots of total Akt and p-Akt (Ser473) following 24 h stimulation of $CD19^+$ B cells. (Right) Induction of Akt phosphorylation following 24 h stimulation, determined by blot image densitometry normalized relative to GAPDH. Data represent the average ±s.e of 3–4 separate experiments.

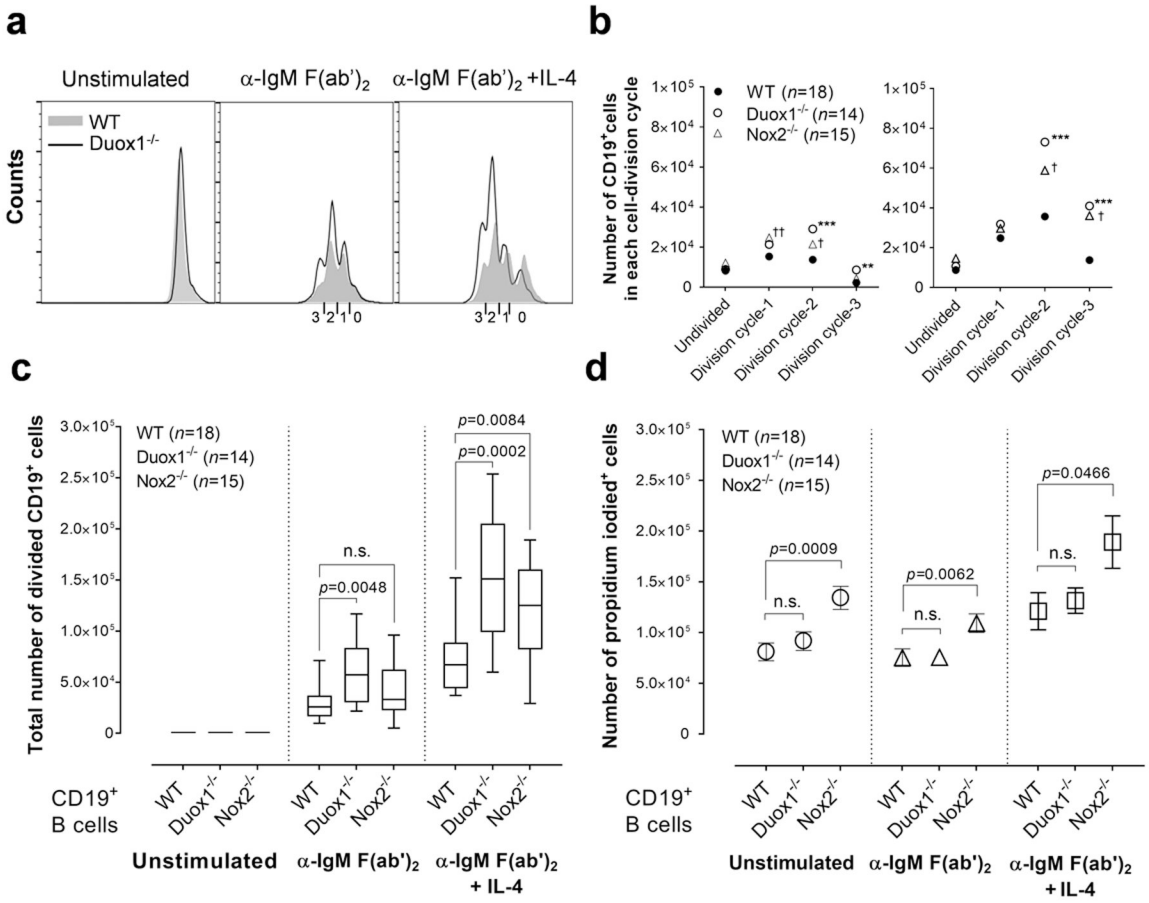

Figure 4.

Duox1 deficiency affects proliferative activity of stimulated splenic CD19$^+$ B cells. (a) Representative CSFE flow cytometric histograms of proliferating CD19$^+$ B cells isolated from WT and Duox1$^{-/-}$ mouse spleen. The cells were cultured with or without 5 μg/ml of anti-IgM F(ab')$_2$ and/or 20 ng/ml of IL-4 for 72 h and their proliferative status was analyzed by dilution of CFSE fluorescence. Each cell division cycle is specified by numbers given below peaks. 0, undivided cell population; 1, division cycle 1; 2, division cycle 2; and 3, division cycle 3. (b) Comparison of cell numbers in each cell cycle division of WT, Duox1$^{-/-}$and Nox2$^{-/-}$ CD19$^+$ B cells. Precise cell numbers were calculated by normalizing with counting microbeads. Each plot is expressed as median of results from individual numbers of each strain. $^{**}p < 0.01$ and $^{***}p < 0.001$ for the test of WT vs Duox1$^{-/-}$. † $p <$ 0.05 and †† $p <$ for the test of WT vs Nox2$^{-/-}$ (two-way ANOVA). (c) Total number of divided CD19$^+$ B cells of WT, Duox1$^{-/-}$ or Nox2$^{-/-}$ mice. Actual cell numbers were calculated by normalizing with counting microbeads. Data are expressed as box-and-whisker plots with median and quartile deviation. Individual number of three strains for the analyses and statistical p value are shown. n.s., not significant difference (Kruskal-Wallis test). (d) Actual number of PI$^+$ events in stimulated cultures. Data are shown as mean ±s.e. of result with statistical p values from individual numbers of each strain. n.s., not significant difference (Kruskal-Wallis test).

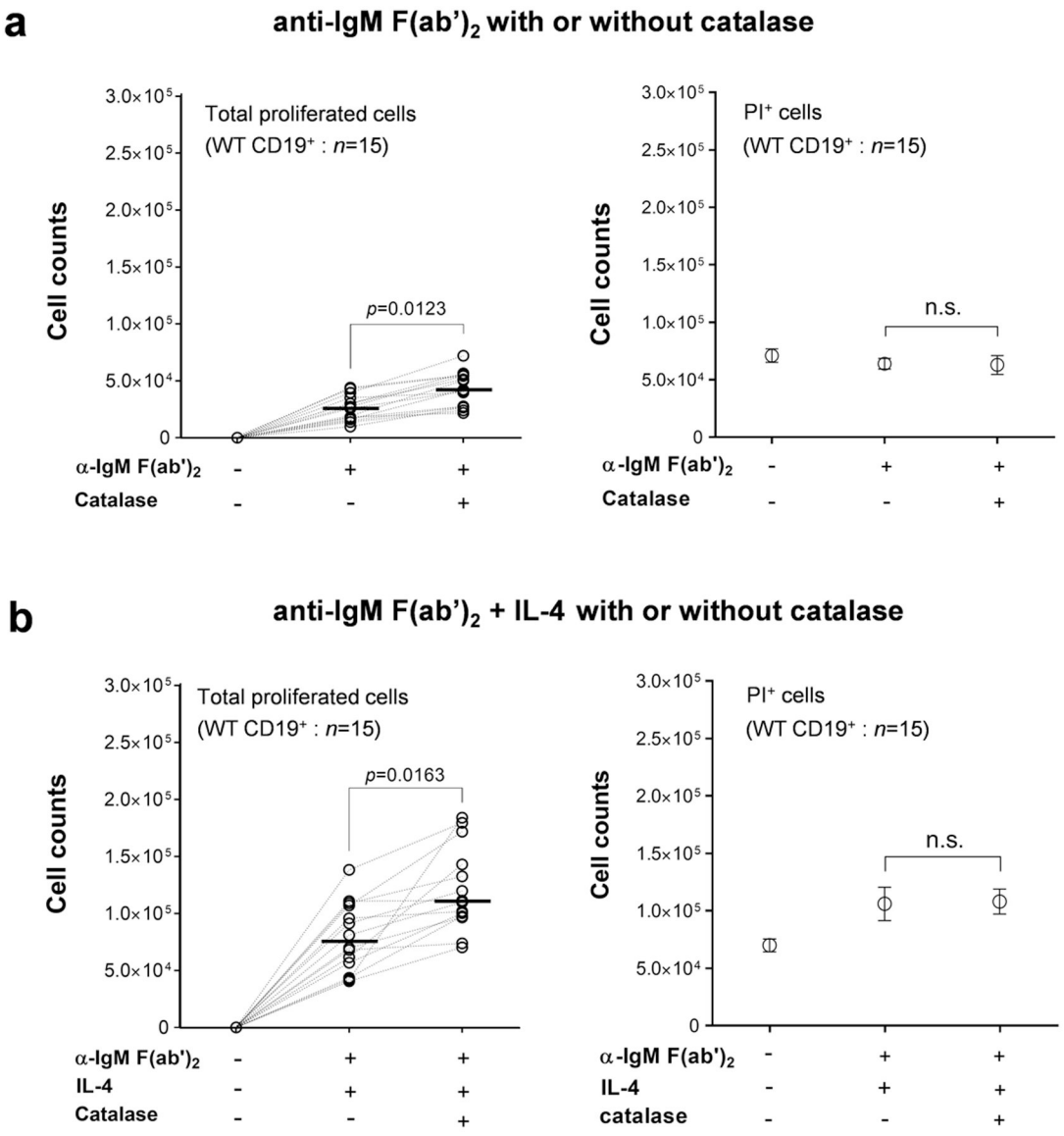

Figure 5.

Enhanced proliferation of WT CD19$^+$ B cells by scavenging of H_2O_2. CD19$^+$ B cells isolated from WT mice were co-cultured with 5 μg/ml of anti-IgM F(ab')$_2$ in the presence (a) or absence (b) of IL-4 (20 ng/ml), either with or without 1 unit/ml of catalase for 72 h. Proliferative activity was compared by CFSE-staining methodology. Actual cell numbers of total divided CD19$^+$ B cells are shown with median, along with lines tracing changes in individual cultures following treatments. Propidium iodide$^+$ (PI$^+$) staining events during the proliferation are expressed as mean ±s.e. n.s., not significant difference (Friedman test).

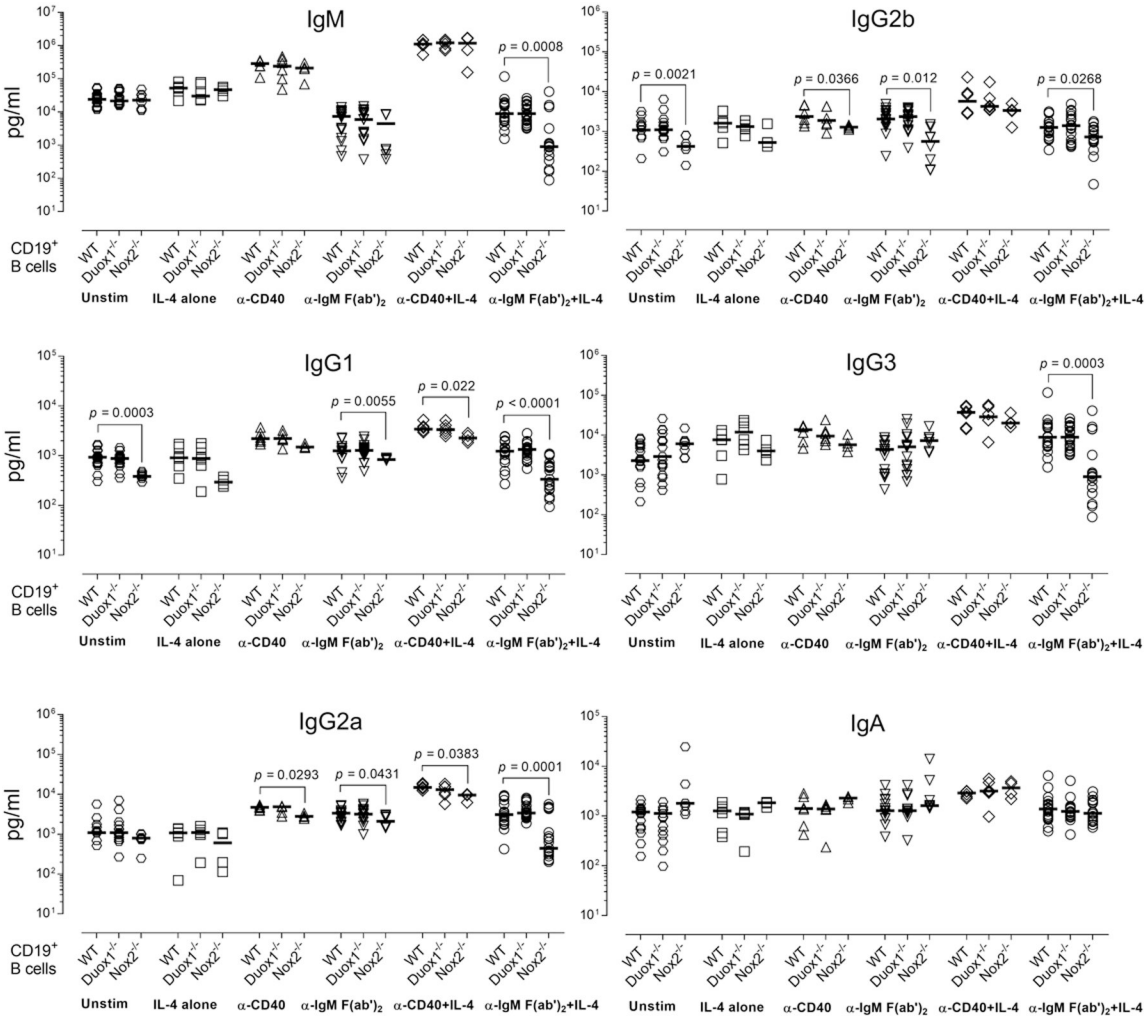

Figure 6.

Duox1-deficient splenic CD19^{+} B cells secrete normal levels of Ig isotypes *in vitro*. CD19^{+} B cells isolated from WT, Duox1$^{-/-}$ or Nox2$^{-/-}$ mice were cultured with each stimulus as indicated in the graph for 3 days. Secretion of 6 major Ig isotypes into the culture media was measured with ELISA. Data are expressed as median values from 6–21 mice of each strain. n.s., not significant differences (Kruskal-Wallis test).

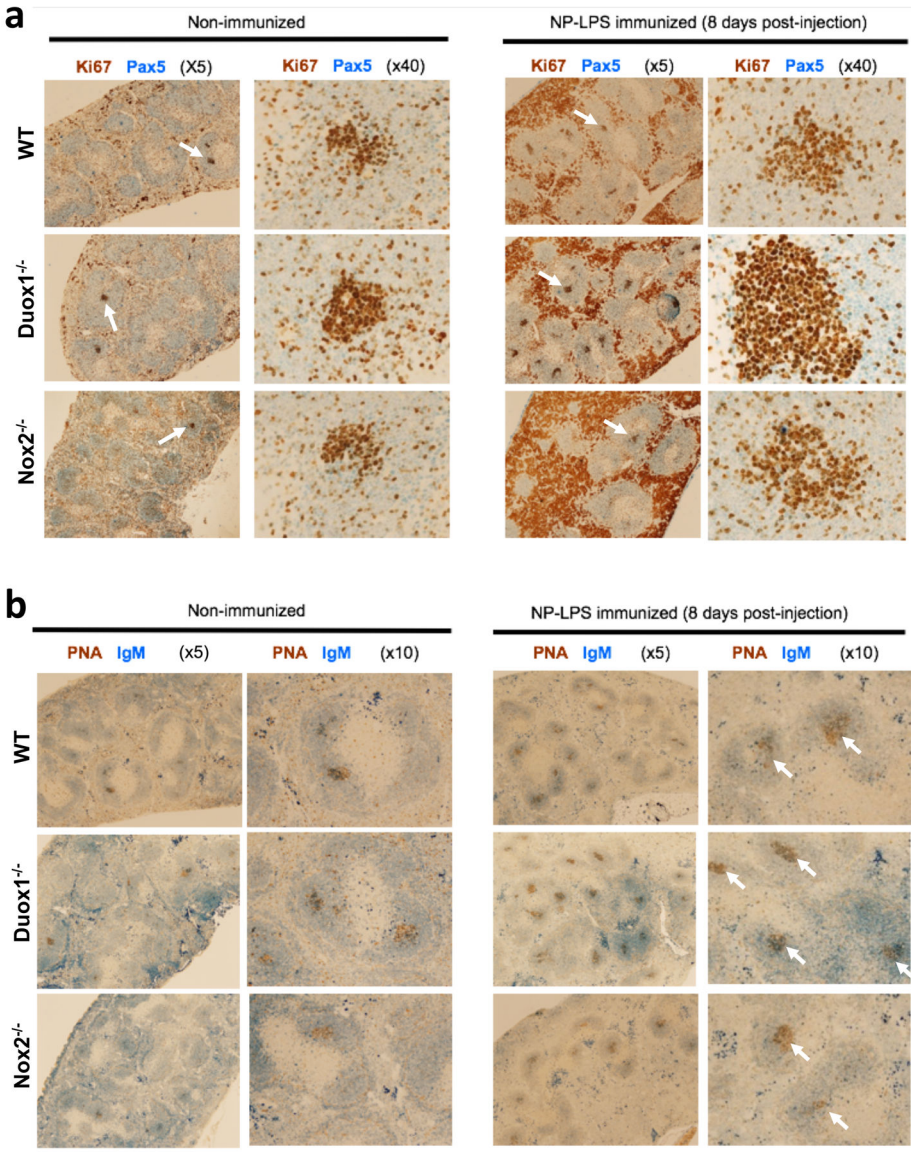

Figure 7.

Immunohistological detection of B cell responses *in vivo* in spleens following immunization. WT, Duox1$^{-/-}$ and Nox2$^{-/-}$ mice were injected with NP-LPS, and then spleens were harvested at 8 days after the immunization. Immunohistochemistry was performed on spleen sections by immune-peroxidase and –phosphatase labeling of (a) anti-Ki67 (brown) and anti-Pax5 (blue), respectively, or (b) PNA (brown) and anti-IgM (blue), respectively. Ki67^{+} proliferating GC cell clusters are indicated with white arrows in (a), whereas PNA reactive GCs are marked with white arrows in (b). Data shown are representative of sections analyzed from 3 mice of each genotype.

Table 1.

Histological evaluation of lymphoid tissue (GCs)

	Strains	Follicle	Numbers of GC	GC reaction	GC proliferation	T cell zone	Marginal zone
	WT	+	7	+	+	+	+
Non-immunized (*n*=3, each)	Duox1$^{-/-}$	+	9	+	+	+	+
	Nox2$^{-/-}$	+	8	+	+.	+	+
	WT.	++	21	++	++	+	+
NP-LPS-immunized (*n*=3, each)	Duox1$^{-/-}$	++	32	+++	+++	+	+
	Nox2$^{-/-}$	++	20	++	++	+	+

Histological marker scoring criteria:

Follicle (IgM, B200): + = normal, ++ = mild proliferation, +++ = moderate

Number of GC (PNA): + = 7–9, ++ = 20 or more, +++ = more than 30

GC reaction (PNA): + = normal, ++ = moderate, +++ = strong reaction

GC proliferation (Ki67): normal, ++ = mild proliferation, +++ = moderate

T cell zone (CD-4): + = normal, ++ = mild activity, +++ = moderate

Marginal zone (B220): + = normal, ++ = mild expansion, +++ = moderate